

# High-efficiency continuous multiple-quantum-well red AlGaInP $\mu$ LED with reduced crosstalk for AR light engines

Yizhou Qian, SID Student Member<sup>1</sup>  | Seok-Lyul Lee, SID Fellow<sup>2</sup>  | Shin-Tson Wu, SID Fellow<sup>1</sup>

<sup>1</sup>College of Optics and Photonics,  
University of Central Florida, Orlando,  
Florida, USA

<sup>2</sup>AUO Corporation, Hsinchu Science Park,  
Hsinchu, Taiwan

## Correspondence

Shin-Tson Wu, College of Optics and  
Photonics, University of Central Florida,  
Orlando, Florida 32816, USA.

Email: [swu@ucf.edu](mailto:swu@ucf.edu)

## Abstract

We develop both electrical and optical models to optimize the light efficiency and minimize the crosstalk of continuous multiple-quantum-well (CMQW) red AlGaInP  $\mu$ LED with a 2.4- $\mu$ m pixel size for augmented reality (AR) applications. Our simulation results agree with the reported experimental data well. We also analyze the physical mechanisms and propose two methods to improve light extraction efficiency (LEE). By redirecting the reflected wave and implementing meta-atoms in the device structure, the LEE of CMQW red AlGaInP  $\mu$ LED is improved by  $\sim 30\%$  while suppressing the crosstalk between adjacent pixels. In addition, by implementing a carbon black matrix, the crosstalk is reduced by  $\sim 5x$  while keeping a relatively high efficiency. As a result, the image blur is alleviated, and image quality is significantly improved. These high-efficiency red  $\mu$ LEDs will help reduce the power consumption of emerging full-color AR glasses.

## KEYWORDS

augmented reality, micro-LED

## 1 | INTRODUCTION

Microscale light-emitting diode ( $\mu$ LED) is a strong contender for augmented reality (AR) light engines due to their high peak luminance, compact form factor, excellent image quality, and long lifetime.<sup>1–3</sup> However, as the chip size decreases, the light emission efficiency decreases because of the surface defects. Presently, full-color, high resolution-density  $\mu$ LED based AR glasses experience a relatively low optical efficiency, especially for red AlGaInP  $\mu$ LEDs,<sup>4,5</sup> which in turn leads to increased power consumption and low ambient contrast ratio, especially under intense ambient lighting conditions.<sup>6,7</sup> For traditional isolated red  $\mu$ LED chips, applying surface passivation and wet etching can alleviate this issue; however, the tradeoffs are reduced emission area and increased nonuniformity.<sup>8</sup> Alternatively, the InGaN-based red  $\mu$ LEDs have a smaller size effect, but their

external quantum efficiency (EQE) remains low due to significant carrier localization arising from high Indium content.<sup>9,10</sup> Moreover, their relatively broad luminescence spectrum significantly reduces the color gamut.<sup>11</sup> On the other hand, InGaN nanowire LED can achieve a peak EQE over 8%, but the demanding bottom-up fabrication procedure limits the manufacturing yield at the current stage.<sup>12</sup> Finally, the cadmium-based quantum dot color-conversion layer can achieve 40% conversion efficiency, but the inadequate photo and thermal stabilities limit their practical applications.<sup>13,14</sup>

Recently, JBD introduced a continuous multiple-quantum-well (CMQW) red AlGaInP  $\mu$ LED.<sup>15</sup> The device structure is depicted in Figure 1. Unlike the pixelated chips, the active region of the CMQW  $\mu$ LED extends across the entire panel, avoiding etching damage to the active layers. With respect to traditional AlGaInP  $\mu$ LED with 2.4- $\mu$ m pixel size, such a new structure boosts the

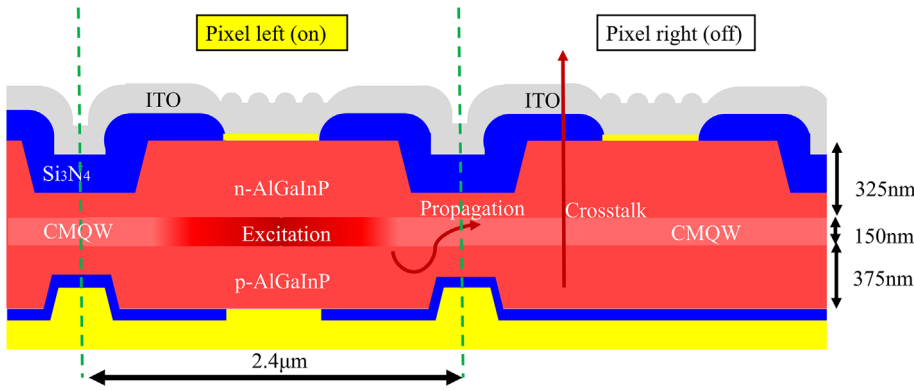


FIGURE 1 Schematic of CMQW  $\mu$ LED structure and optical crosstalk.

efficiency by  $3.5\times$ . Despite these advancements, CMQW  $\mu$ LEDs still face significant challenges. First, the low light extraction efficiency (LEE) in red AlGaInP  $\mu$ LEDs remains to be overcome.<sup>16</sup> The large refractive index mismatch between AlGaInP and the dielectric passivation layer or indium tin oxide (ITO) causes the emitted light to be trapped within the structure, eventually being absorbed by metal contacts or the absorptive AlGaInP material. Second, due to the limited etching accuracy, a minimum of 300-nm thick AlGaInP, including the active region, must remain connected between adjacent pixels. This connection leads to electrical and optical crosstalk: current diffusion can induce unwanted excitation in neighboring pixels, and the CMQW structure can act as a waveguide, causing light leakage into adjacent pixels.<sup>4</sup> Such crosstalk causes image blur, which in turn degrades image fidelity.

In this paper, we simulate and evaluate both the electrical and optical performance of CMQW red  $\mu$ LEDs. Our results agree well with the measured data reported by JBD, validating our simulation model. Next, we analyze the loss mechanisms within the CMQW structure and propose practical solutions compatible with current fabrication capabilities. By redirecting reflected waves and implementing meta-atoms, we optimize the device structure and increase the effective LEE from 6.4% to 8.3%. In the meantime, crosstalk between adjacent pixels is reduced from 19.5% to 15%. By implementing a carbon black matrix (BM), the crosstalk is further reduced to 3.8%, corresponding to a  $5\times$  improvement, while the effective LEE remains at 6.9%, which is still higher than that of an unoptimized device. This significantly reduced crosstalk helps enhance overall image quality and minimize image blur.

## 2 | MODELING AND METHOD

### 2.1 | CMQW structure and crosstalk

Figure 1 describes the CMQW  $\mu$ LED structure with a 2.4- $\mu$ m pixel size based on JBD's SEM image.<sup>15</sup> From

bottom to top, the structure is composed of metal bonding layer Au, p-electrode Au with a diameter of 625 nm, 50-nm thick dielectric passivation layer  $\text{Si}_3\text{N}_4$ , 375-nm p-AlGaInP, 100-nm active region with 5 pairs of MQW, 325-nm n-AlGaInP, 150-nm thick dielectric passivation layer  $\text{Si}_3\text{N}_4$ , 10-nm thick Au/Ni n-electrode with diameter of 700 nm, and 300-nm thick ITO. A hemisphere grating with a diameter of 150 nm and periodicity of 200 nm is placed on top of the ITO layer to increase the LEE.

Here, we first consider two pixels: the left pixel is turned on and the right pixel is turned off. When the active region of the left pixel is activated, electron-hole recombination takes place in the CMQW. If the current diffusion is too strong, the electron-hole recombination can also take place in the right pixel. More importantly, optical crosstalk due to 1) electrical crosstalk and 2) light propagation as waveguide mode, as indicated by the red arrows, in the CMQW  $\mu$ LED structure may cause significant image quality degradation.<sup>17</sup>

### 2.2 | Electrical simulation of CMQW $\mu$ LED

Silvaco TCAD (Silvaco Inc., Santa Clara) is employed to perform 2D CMQW  $\mu$ LED simulation. As shown in Figure 2A, three adjacent pixels are considered for evaluating the electrical performance and crosstalk. As reported by JBD, the total thickness of CMQW  $\mu$ LED is below 1  $\mu$ m. To achieve such a thin film, the AlGaInP  $\mu$ LED needs to be polished. In our simulation, the P-type AlGaInP layer is Mg-doped and the N-type AlGaInP layer is Si-doped with both doping concentrations of  $10^{19}\text{ cm}^{-3}$ . In the active region, the bandgap of AlGaInP is dependent on the Al, Ga, and In compositions.

To obtain a 620 nm peak wavelength, we apply  $\text{Al}_{0.15}\text{Ga}_{0.3}\text{In}_{0.55}\text{P}$  in the MQW and the full-width-at-half-maximum is only 18 nm as shown in Figure 2B. To

FIGURE 2 (A) CMQW electrical model in Silvaco TCAD. (B) Simulated normalized emission spectra. (C) Simulated normalized radiative recombination rate.

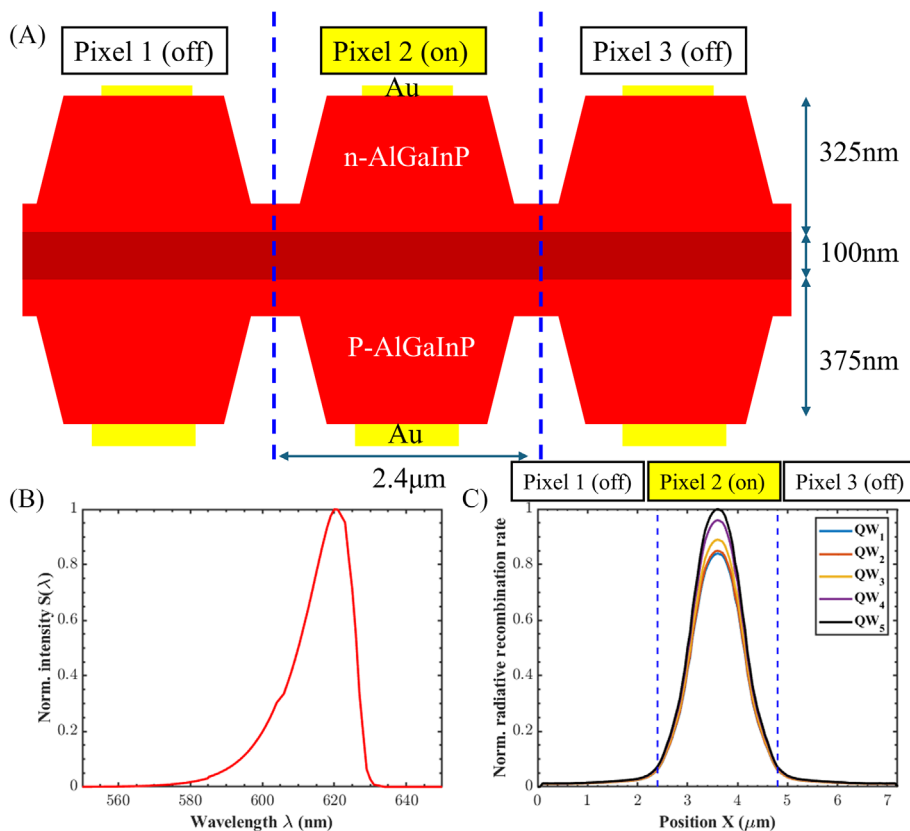
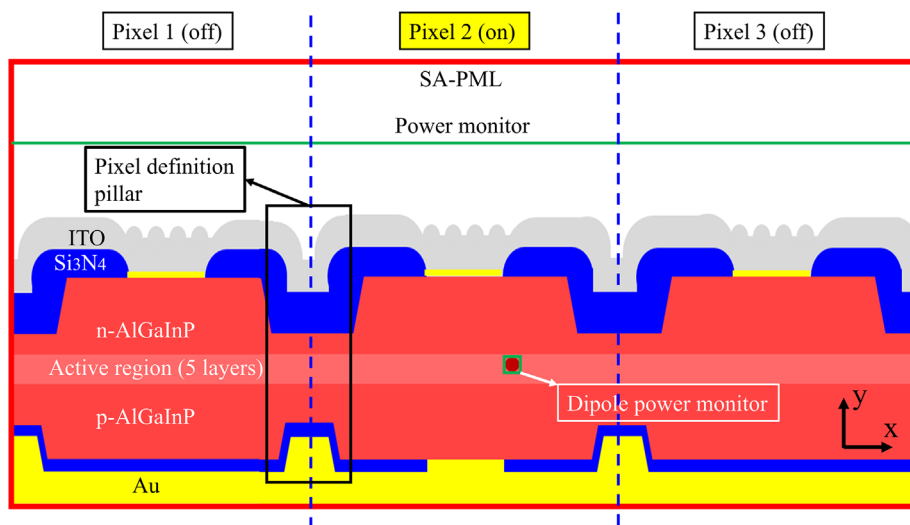


FIGURE 3 Schematic of 2D-FDTD CMQW  $\mu\text{LED}$  simulation model.



increase the quantum confinement, we applied  $(\text{Al}_{0.5}\text{Ga}_{0.5})_{0.52}\text{In}_{0.48}\text{P}$  as a quantum barrier whose energy gap is approximately 2.2 eV.<sup>18</sup> Figure 2C indicates the normalized radiative recombination rate in the active region when the current density is  $30\text{A}/\text{cm}^2$  and the applied voltage is  $\sim 2.0$  V. Although the electrical crosstalk to adjacent pixels is only 7%, the excitation of dipoles close to adjacent pixels still induces some optical crosstalk.

### 2.3 | Optical simulation of CMQW microLED

The red CMQW AlGaInP  $\mu\text{LED}$  model is built in the 2D finite-difference time-domain (FDTD, Ansys) software as depicted in Figure 3. A total of three pixels are simulated to calculate the optical crosstalk and the total simulation region width is 9  $\mu\text{m}$ . On top of each pixel, a photonic crystal with 140 nm diameter and

200 nm periodicity is laminated on the top surface of the ITO electrode. The top Au electrode is thinned to 9 nm to ensure high transparency,<sup>19</sup> and the Si<sub>3</sub>N<sub>4</sub> dielectric passivation layer is applied on both sides of the CMQW  $\mu$ LED to avoid conductivity. Between adjacent pixels, trapezoidal bottom metallic and inverted trapezoidal top dielectric pixel definition pillars are applied to reduce optical crosstalk. The dispersion of all the materials is considered.<sup>16</sup> The whole structure is immersed in polyimide whose refractive index is 1.5 and the boundary condition is the steep-angle perfect matched layer (SA-PML). A power monitor is placed on top of the structure to calculate the emission power and optical crosstalk. Small box monitors are placed surrounding each dipole source to receive the dipole power.

To precisely calculate the optical response, we applied a dipole cloud in the simulation model. In the vertical (y) direction, a total of 5 dipoles are simulated for 5 pairs of QW. In the horizontal (x) direction, a total of 25 dipoles are included and each dipole is spaced at 50 nm. For the zincblende crystal structure, the dipoles oscillate equally in all directions. Therefore, dipoles oscillate along all the x-, y-, and z-directions need to be considered. To avoid confusion with the dipole position (x, y), we denote the dipole oscillation directions to be (X, Y, Z). Although AR optics typically have an acceptance cone limited to  $\pm 20^\circ$ , integrating a microlens array can effectively reshape the CMQW  $\mu$ LED's emission pattern, allowing for efficient light extraction from a broader range of angles.<sup>3</sup> Therefore, in this paper, we focus on optimizing the light emissions from all angles. The LEE of each dipole can be calculated as the power ratio between the power monitor to the dipole box monitor<sup>20</sup>:

$$LEE_d(X, Y, Z, x, y) = \frac{\int_{-1.2\mu\text{m}}^{1.2\mu\text{m}} \int_{-4.5\mu\text{m}}^{4.5\mu\text{m}} P_E(X, Y, Z, x, y, \lambda) S(\lambda) dW d\lambda}{\int P_D(X, Y, Z, x, y, \lambda) S(\lambda) d\lambda}, \quad (1)$$

where  $P_E$  and  $P_D$  represent the power received by the planar power monitor and box dipole monitor, respectively,

and  $S(\lambda)$  is the emission spectrum. However, due to optical crosstalk, the light emitted from adjacent pixels is considered as stray light. Therefore, we define  $LEE_d'$  as the effective LEE where the light emits from the original pixel:

$$LEE_d'(X, Y, Z, x, y) = \frac{\int_{-1.2\mu\text{m}}^{1.2\mu\text{m}} \int_{-4.5\mu\text{m}}^{4.5\mu\text{m}} P_E(X, Y, Z, x, y, \lambda) S(\lambda) dW d\lambda}{\int P_D(X, Y, Z, x, y, \lambda) S(\lambda) d\lambda}, \quad (2)$$

The position dependence can be eliminated by considering electrical weightage:

$$LEE'(X, Y, Z) = \frac{\sum_{y=1}^5 \int_{-4.5\mu\text{m}}^{4.5\mu\text{m}} LEE_d'(X, Y, Z, x, y) E(x, y) dx}{\sum_{y=1}^5 \int_{-4.5\mu\text{m}}^{4.5\mu\text{m}} E(x, y) dx}, \quad (3)$$

where  $E(x, y)$  is position-dependent normalized radiative recombination rate as shown in Figure 2C. The final LEE result is the average of dipoles oscillating in all directions. The LEE' results for (X, Y, Z) dipoles are 9.1%, 0.6%, and 9.5%, respectively. The LEE' for the Y-oscillating dipole is significantly lower than that of the other two dipoles because the emitted power is the strongest along the x-direction. The overall LEE' is 6.4%.

To calculate the crosstalk of the CMQW structure, the electrical and optical weights of all the dipoles need to be considered. The total crosstalk can be calculated as:

$$Crosstalk(X, Y, Z) = \frac{\int_{-1.2\mu\text{m}}^{1.2\mu\text{m}} \int_{-4.5\mu\text{m}}^{4.5\mu\text{m}} \sum_{y=1}^5 P_E(X, Y, Z, x, y, W) LEE_d'(X, Y, Z, x, y) E(x, y) dx dW}{\int_{-4.5\mu\text{m}}^{4.5\mu\text{m}} \int_{-4.5\mu\text{m}}^{4.5\mu\text{m}} \sum_{y=1}^5 P_E(X, Y, Z, x, y, W) LEE_d'(X, Y, Z, x, y) E(x, y) dx dW}. \quad (4)$$

Figure 4 shows that the total crosstalk of the CMQW  $\mu$ LED is 19.5%, which agrees well with the measured data by JBD. The crosstalk of the (X, Y, Z) dipoles is 23%, 53%, and 17%, respectively. The Y-oscillating dipole exhibits a noticeably higher crosstalk than the other two. However, because the associated LEE is low, it does not make a significant impact on the total result.

### 3 | DISCUSSION AND OPTIMIZATION

#### 3.1 | Optical losses in CMQW structure

Due to the CMQW structure, the  $\mu$ LED behaves like a waveguide. At the same time, due to the existence of a pixel definition pillar, the  $\mu$ LED also behaves like a quasi-cavity. There are three ways to improve the EQE in such a structure as indicated in Figure 5A. The first method is to modify the position of the CMQW to

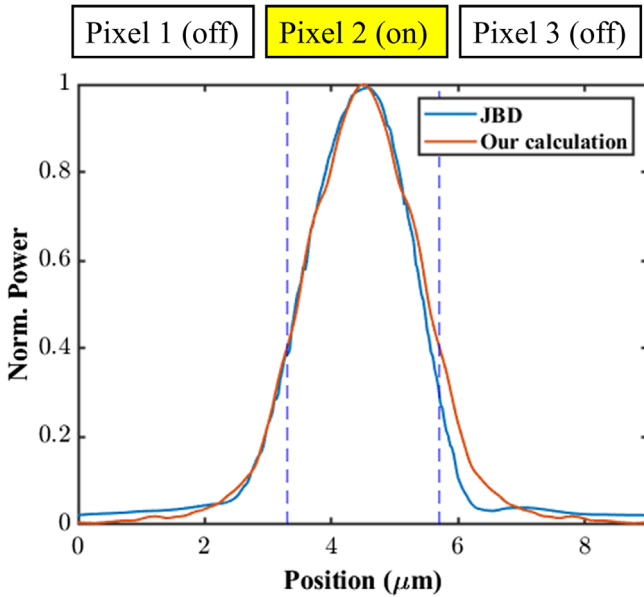


FIGURE 4 Comparison between simulated crosstalk and the measured data by JBD.<sup>15</sup>

improve the constructive interference in the waveguide to increase the air mode and reduce the waveguide mode. However, the geometrical freedom in thin-film CMQW structure is limited because the pixel definition pillar needs to be placed far from the active layer, especially when the CMQW thickness is merely 100 nm. By sweeping the p-AlGaInP thickness from 350 nm to 500 nm with a 10-nm step, the LEE of 5 pairs MQW only slightly fluctuates between 6.2% and 6.5%. The second method is to redirect the waveguide mode by optimizing the pixel definition layer as Figure 5B shows. For the bottom  $\text{Si}_3\text{N}_4$  coated metallic layer, the height of the layer ( $H_B$ ) is fixed at 200 nm, while the tilt angle is modulated by the length ( $L_B$ ). Similarly, for the top dielectric pixel definition pillar, the tilt angle is controlled by  $L_T$ .

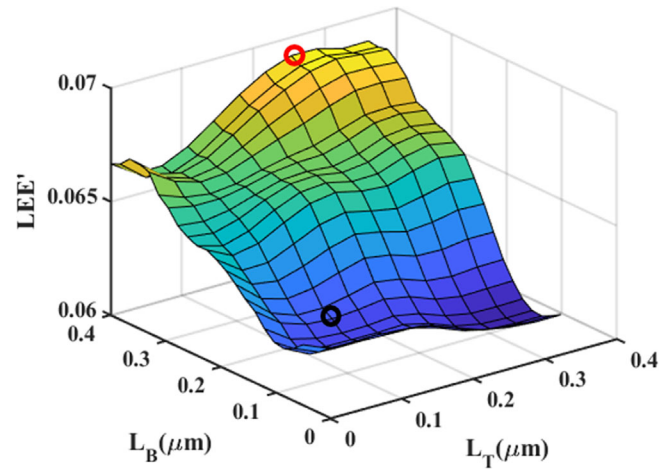


FIGURE 6 Colormap of  $LEE'$  as a function of  $L_T$  and  $L_B$ . black circle:  $LEE'$  before optimization. Red circle:  $LEE'$  after optimization.

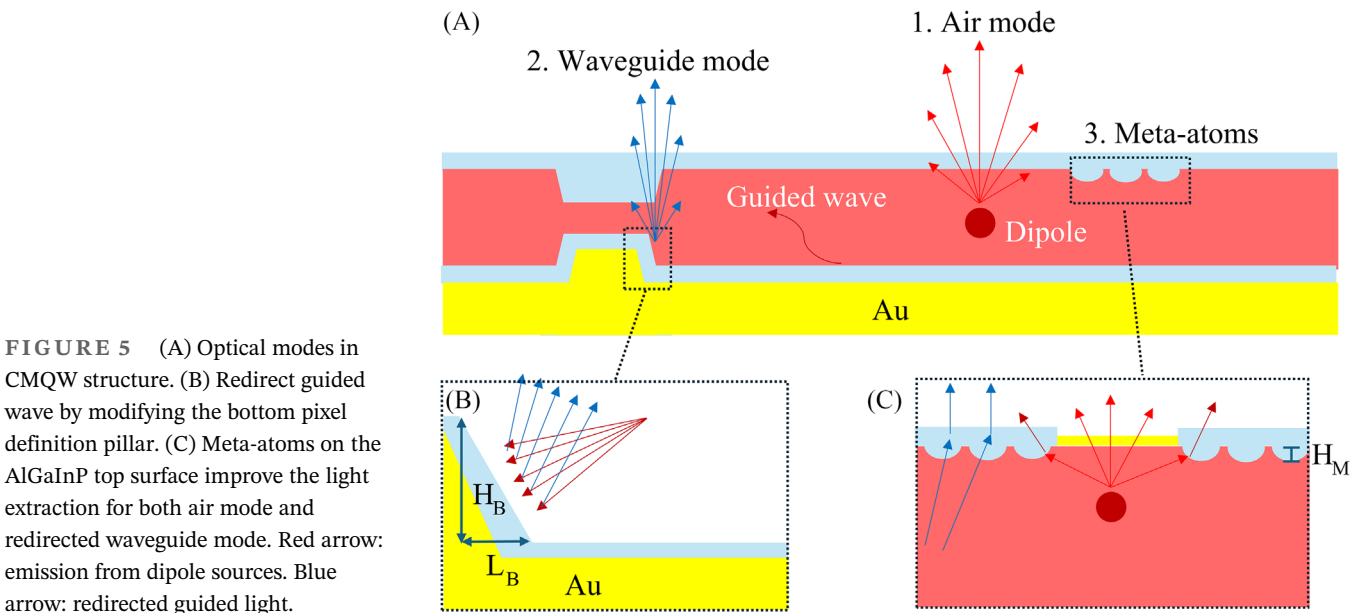


FIGURE 5 (A) Optical modes in CMQW structure. (B) Redirect guided wave by modifying the bottom pixel definition pillar. (C) Meta-atoms on the AlGaInP top surface improve the light extraction for both air mode and redirected waveguide mode. Red arrow: emission from dipole sources. Blue arrow: redirected guided light.

### 3.2 | Optimization

Figure 6 indicates the optimized LEE results by sweeping both  $L_T$  and  $L_B$  from 0 to  $0.4 \mu\text{m}$ . Limited by computer memory, we only considered dipoles placed in the center of each pixel. In the vertical direction, 5 dipoles are considered to average out the interference effect. The black dot indicates that  $LEE' = 6.2\%$  before optimization when  $L_T = 0.1 \mu\text{m}$  and  $L_B = 0.14 \mu\text{m}$ . By increasing  $L_T$  to  $0.25 \mu\text{m}$  and  $L_B$  to  $0.4 \mu\text{m}$ ,  $LEE'$  increases to  $6.9\%$ , corresponding to an 11% improvement.

The improvement by modulating the pixel definition pillar is limited because most of the light is still trapped in the structure due to the large refractive index differences

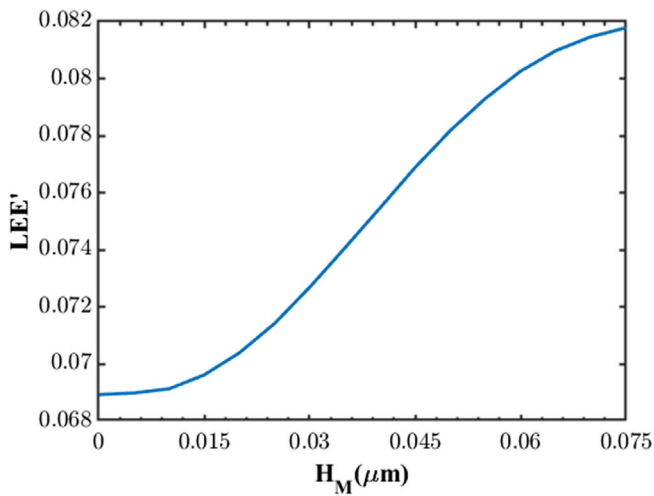


FIGURE 7 Simulated  $LEE'$  as a function of moth-eye structure depth ( $H_M$ ).

between AlGaInP and  $\text{Si}_3\text{N}_4$ . To improve the light extraction, we consider the third method which incorporates meta-atoms at the interfaces between AlGaInP and  $\text{Si}_3\text{N}_4$  as shown in Figure 5C. The moth-eye-like antireflection film helps increase the light transmittance without inducing electrical conductivity issues.<sup>21</sup> However, due to the existence of the thin metallic electrode, the center of the pixel does not contain moth-eye meta-atoms. In our optimization, we fix the periodicity of the moth-eye structure at  $150 \text{ nm}$  and the diameter at  $150 \text{ nm}$ . Figure 7 depicts the sweeping results by increasing the moth-eye structure depth ( $H_M$ ) from 0 to  $75 \text{ nm}$ . The  $LEE'$  further increases from  $6.9\%$  to  $8.2\%$ , corresponding to another 19% improvement. By combining both methods, the  $LEE'$  of the 5-layer center dipoles increases from  $6.2\%$  to  $8.2\%$ , corresponding to a total improvement of 32%.

Based on the obtained geometrical values, we used a dipole cloud to simulate the optimized CMQW  $\mu\text{LED}$  structure. The  $LEE'$  of the dipole cloud increases from  $6.4\%$  to  $8.3\%$ , which is improved by  $\sim 30\%$ . We notice that the improvement for the dipole cloud is slightly lower than the center dipoles because the redirection of the pixel definition pillar is optimized for the center dipoles instead of the edge dipoles. However, the total crosstalk only slightly improves from  $19.5\%$  to  $15\%$  with a narrower line shape.

### 3.3 | Minimizing crosstalk

As shown in Figure 8, the optical crosstalk can be suppressed by implementing a black matrix (BM) on the top of pixel definition pillar. Such carbon BM structure can be fabricated by inkjet printing or by photolithography. We

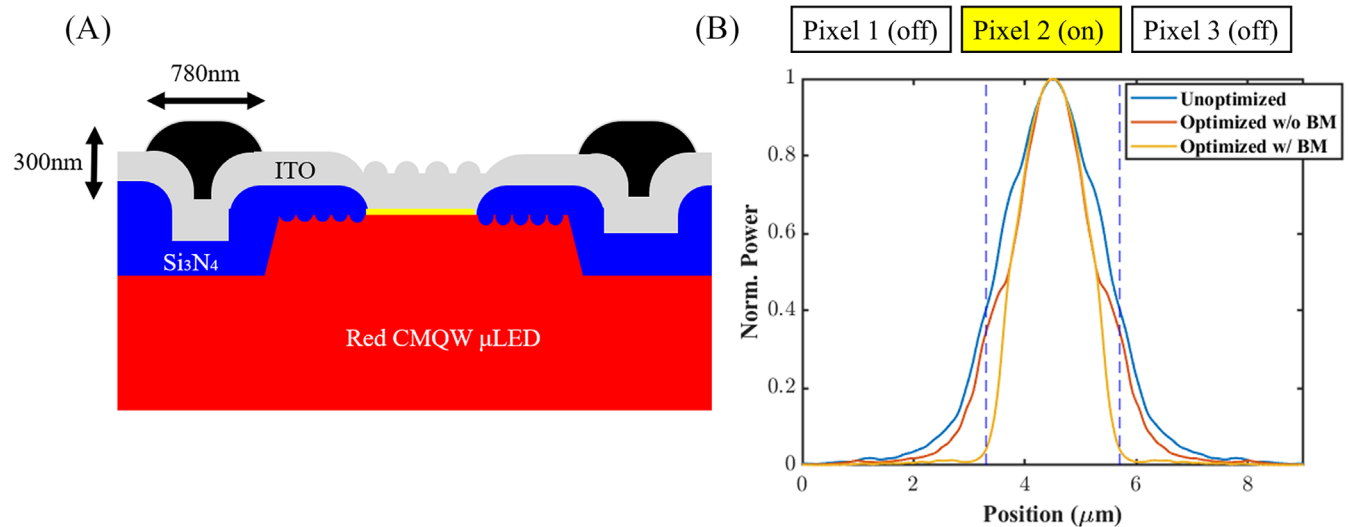
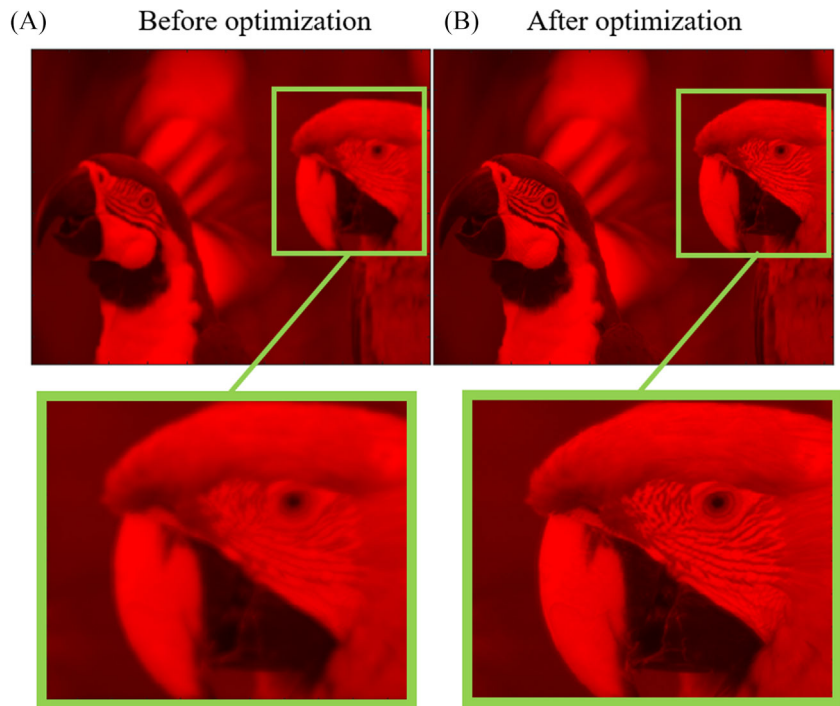


FIGURE 8 (a) Schematic of red CMQW  $\mu\text{LED}$  with black matrix on top of the pixel definition pillar. (b) Comparison of simulated crosstalk between unoptimized and optimized CMQW  $\mu\text{LED}$ s with and without black matrix.

FIGURE 9 Simulated image of CMQW red  $\mu$ LED (A) without BM and (B) with BM.



have considered the dispersion of carbon black, and its refractive index is  $1.8 + 0.7i$  at  $\lambda = 620$  nm. After applying BM, the total crosstalk dramatically decreases from 15% to 3.8%. Compared to unoptimized cases (19.5%), the total crosstalk is suppressed by  $\sim 5x$ . Due to the absorption of the black matrix, the  $LEE'$  decreases to 6.9%, which is still better than the unoptimized case, which is 6.4%. By using a higher absorptive material such as a Ta-doped black matrix, the total crosstalk can be further reduced to 2.8%, but the cost will increase.

### 3.4 | Image quality

Figure 9 demonstrates the improved image quality achieved by incorporating carbon BM. As shown in Figure 9A, a high crosstalk level of 19.5% introduces noticeable image blurs, particularly in the regions containing sufficient details. By reducing the crosstalk to 3.8%, the image quality is significantly enhanced (Figure 9B). This improvement is reflected in the multi-scale structural similarity index,<sup>22</sup> which increases from 0.978 to 0.987 after optimization, indicating a closer match to the original image.

## 4 | CONCLUSION

We have successfully optimized the CMQW red AlGaInP  $\mu$ LEDs by modifying the pixel definition pillar and

implementing moth-eye meta-atoms. These optimization processes increase the LEE from 6.4% to 8.3%, representing an improvement of  $\sim 30\%$ . Additionally, the overall crosstalk between adjacent pixels is reduced from 19.5% to 15%. By implementing BM, the crosstalk is further decreased to 3.8%, while keeping a high LEE of 6.9%. This significant reduction in crosstalk enhances the overall image quality and minimizes the image blurs. Further enhancement can be achieved by controlling current diffusion and optimizing the meta-atom structures. The development of these high-efficiency, low-crosstalk red AlGaInP  $\mu$ LEDs can significantly reduce power consumption and improve the image quality of AR glasses.

### ORCID

Yizhou Qian  <https://orcid.org/0000-0002-2157-0497>  
Seok-Lyul Lee  <https://orcid.org/0000-0002-3754-826X>

### REFERENCES

- Lin CC, Wu YR, Kuo HC, Wong MS, DenBaars SP, Nakamura S, et al. The micro-LED roadmap: status quo and prospects. *J Phys Photonics*. 2023;5(4):042502. <https://doi.org/10.1088/2515-7647/acf972>
- Huang Y, Hsiang EL, Deng MY, Wu ST. Mini-LED, micro-LED and OLED displays: present status and future perspectives. *Light Sci Appl*. 2020;9(1):105. <https://doi.org/10.1038/s41377-020-0341-9>
- Hsiang EL, Yang Z, Yang Q, Lai PC, Lin CL, Wu ST. AR/VR light engines: perspectives and challenges. *Adv Opt Photonics*. 2022;14(4):783–861. <https://doi.org/10.1364/AOP.468066>

4. Hsiang EL, Yang Z, Yang Q, Lan YF, Wu ST. Prospects and challenges of mini-LED, OLED, and micro-LED displays. *J Soc Inf Disp*. 2021;29(6):446–65. <https://doi.org/10.1002/jsid.1058>
5. Fan K, Tao J, Zhao Y, Li P, Sun W, Zhu L, et al. Size effects of AlGaInP red vertical micro-LEDs on silicon substrate. *Results Phys*. 2022;36:105449. <https://doi.org/10.1016/j.rinp.2022.105449>
6. Qian Y, Yang Z, Hsiang EL, Yang Q, Nilsen K, Huang Y-H, et al. Human eye contrast sensitivity to vehicle displays under strong ambient light. *Crystals*. 2023;13(9):1384. <https://doi.org/10.3390/cryst13091384>
7. Qian Y, Chen SC, Hsiang EL, Akimoto H, Lin C-L, Wu S-T. Enhancing a Display's sunlight readability with tone mapping. *Photonics*. 2024;11(6):578. <https://doi.org/10.3390/photonics11060578>
8. Wong MS, Lee C, Myers DJ, Hwang D, Kearns JA, Li T, et al. Size-independent peak efficiency of III-nitride micro-light-emitting-diodes using chemical treatment and sidewall passivation. *Appl Phys Express*. 2019;12(9):097004. <https://doi.org/10.7567/1882-0786/ab3949>
9. Flemish J, Armitage R, Ren Z, Soer W, Lotfi H, Chung T, et al. 38–3: invited paper: MicroLED device technology for low-power wearable displays. *SID Symp Digest Tech Papers*. 2022; 53(1):478–80. <https://doi.org/10.1002/sdtp.15526>
10. Armitage R, Ren Z, Holmes M, Flemish J. True-red InGaN light-emitting diodes for display applications. *Phys Status Solidi RRL*. 2024;18(11):2400012. <https://doi.org/10.1002/pssr.202400012>
11. Robin Y, Pristovsek M, Amano H, Oehler F, Oliver R, Humphreys C. What is red? On the chromaticity of orange-red InGaN/GaN based LEDs. *J Appl Phys*. 2018;124(18):183102. <https://doi.org/10.1063/1.5047240>
12. Pandey A, Xiao Y, Reddeppa M, Malhotra Y, Liu J, Min J, et al. A red-emitting micrometer scale LED with external quantum efficiency > 8%. *Appl Phys Lett*. 2023;122(15):151103. <https://doi.org/10.1063/5.0129234>
13. Liu Z, Lin CH, Hyun BR, Sher CW, Lv Z, Luo B, et al. Micro-light-emitting diodes with quantum dots in display technology. *Light Sci Appl*. 2020;9(1):83. <https://doi.org/10.1038/s41377-020-0268-1>
14. Plante IJL, Barron A, Yamanaga J, Bautista MJ, Tillman J, Wang X, et al. 55–2: invited paper: quantum dot color conversion for displays. *SID Symp Digest Tech Papers*. 2023;54(1):792–4. <https://doi.org/10.1002/sdtp.16681>
15. Li Q, Tan W, Zhu Y, Guo J, Jiang X. 11–1: invited paper: Micro-LED displays for augmented reality smart glasses. *SID Symp Digest Tech Papers*. 2024;55(1):104–7. <https://doi.org/10.1002/sdtp.17464>
16. Gou F, Hsiang EL, Tan G, Chou PT, Li YL, Lan YF, et al. Angular color shift of micro-LED displays. *Opt Express*. 2019; 27(12):A746–57. <https://doi.org/10.1364/OE.27.00A746>
17. Diethelm M, Penninck L, Altazin S, Hiestand R, Kirsch C, Ruhstaller B. Quantitative analysis of pixel crosstalk in AMOLED displays. *J Soc Inf Disp*. 2018;19(2):61–9. <https://doi.org/10.1080/15980316.2018.1428232>
18. Fedorova OA, Bulashevich KA, Karpov SY. Critical aspects of AlGaInP-based LED design and operation revealed by full electrical-thermal-optical simulations. *Opt Express*. 2021; 29(22):35792–805. <https://doi.org/10.1364/OE.443898>
19. Bauch M, Dimopoulos T. Design of ultrathin metal-based transparent electrodes including the impact of interface roughness. *Mater Design*. 2016;104(15):37–42. <https://doi.org/10.1016/j.matdes.2016.04.082>
20. Qian Y, Yang Z, Huang YH, Lin KH, Wu ST. Directional high-efficiency nanowire LEDs with reduced angular color shift for AR and VR displays. *Opto-Electron Sci*. 2022;1(12):220021. <https://doi.org/10.29026/oes.2022.220021>
21. Tan G, Lee JH, Lan YH, Wei MK, Peng LH, Cheng IC, et al. Broadband antireflection film with moth-eye-like structure for flexible display applications. *Optica*. 2017;4(7):678–83. <https://doi.org/10.1364/OPTICA.4.000678>
22. Wang Z, Simoncelli EP, Bovik AC. Multiscale structural similarity for image quality assessment. In *Proceedings of the Thirty Seventh Asilomar Conference on Signals, Systems & Computers* 2003;2:1398–402. <https://doi.org/10.1109/ACSSC.2003.1292216>

## AUTHOR BIOGRAPHIES



**Yizhou Qian** received his B.S. degree from Virginia Tech, Blacksburg, Virginia, USA in 2018 and M.Eng. degree from Virginia Tech, Blacksburg, Virginia, USA in 2021. Currently, he is working toward a Ph.D. degree at the College

of Optics and Photonics, University of Central Florida, Florida, USA. His current research focuses on micro-LED, OLED, and mini-LED backlight LCD for light engines for AR/VR display systems and flat panel displays.



**Seok-Lyul Lee** received his Ph.D. in Photonics from National Yang Ming Chiao Tung University. He is a director and fellow at AUO Corporation. His current research focuses on micro-LED display technology. He invented the fringe-field switching

(FFS) liquid crystal mode, which improved display viewing angles. This innovation was crucial for mobile, tablet, and monitor TFT-LCD products. He received the SID Special Recognition Award in 2012 and was named an SID Fellow in 2018. Since 2019, he has been developing next-generation micro-LED displays. In 2021, he introduced the world's first 9.4-in. 228-ppi flexible micro-LED display, earning the SID Distinguished Paper Award. He is now working on augmented reality (AR) glasses, leveraging his expertise in LCD and micro-LED technology.





**Shin-Tson Wu** is a Trustee Chair professor at the College of Optics and Photonics, University of Central Florida (UCF). He is an Academician of Academia Sinica, a Charter Fellow of the National Academy of Inventors, and a Fellow of the IEEE, OSA, SID, and SPIE. He is a recipient of the SID Lawrence Tannas award (2025), Optica Edwin H. Land Medal (2022), SPIE Maria Goeppert-Mayer Award (2022), Optica Esther Hoffman Beller Medal (2014), SID Slottow-Owaki Prize (2011), Optica Joseph Fraunhofer Award (2010), SPIE G. G. Stokes Award (2008), and SID Jan Rajchman Prize (2008). In the

past, he served as the founding Editor-In-Chief of the Journal of Display Technology, Optica publications council chair and board member, and SID honors and awards committee chair.

**How to cite this article:** Qian Y, Lee S-L, Wu S-T. High-efficiency continuous multiple-quantum-well red AlGaInP  $\mu$ LED with reduced crosstalk for AR light engines. J Soc Inf Display. 2025. <https://doi.org/10.1002/jsid.2063>